Energy, Environmental, and Catalysis Applications

Secondary Sphere Effects on Porous Polymeric Organocatalysts for CO2 Transformations: Subtle Modifications Resulting in Superior Performance

Yanpei Song, Qi Sun, Pui Ching Lan, and Shengqian Ma

ACS Appl. Mater. Interfaces, **Just Accepted Manuscript** • DOI: 10.1021/acsami.0c08817 • Publication Date (Web): 29 Jun 2020

Secondary Sphere Effects on Porous Polymeric Organocatalysts for CO_2 Transformations: Subtle Modifications Resulting in Superior Performance

Yanpei Song,[†] Qi Sun,[*,‡] Pui Ching Lan,[†] and Shengqian Ma[*,†]

[†]Department of Chemistry, University of South Florida, 4202 East Fowler Avenue, Tampa, Florida 33620, United States

[‡]Key Laboratory of Biomass Chemical Engineering of Ministry of Education, College of Chemical and Biological Engineering, Zhejiang University, Hangzhou 310027, P. R. China

KEYWORDS. Porous materials, CO_2 transformation, secondary sphere interaction, organocatalysis, cooperation catalysis

ABSTRACT: Albeit harnessing secondary sphere interactions to exert control over the reaction outcomes has primarily been applied to enzymatic and organometallic catalysis, there are seldom any studies that introduce outer-sphere modifiers into organocatalysts. This is even less in the corresponding heterogeneous catalytic system. In this contribution, we experimentally and computationally investigate the role of secondary effects on the reactivity of bromide anions toward CO_2 transformations. Six pyridinium cationic porous frameworks have been synthesized and fully characterized. Structure-activity relationships and kinetics show that the type and the location of the substituents on the cationic framework have a significant impact on the nucleophilic reactivity of their bromide counter anion. Specifically, the attachment of amine substituent to the ortho position relative to a pyridinium motif produces a remarkably efficient catalyst for CO_2 transformation, by a factor of six times greater in comparison to the pristine pyridinium-based polymer. The hydrogen-bond-interaction-promoted reagent activation and enhanced delocalization ability of bromide counter anion are believed to be the key to driving the reaction towards CO_2 utilization. These observations, therefore, champion the leverage of secondary interaction for optimizing the reactivity of organocatalysts.

INTRODUCTION

The secondary sphere refers to any moiety in the molecular microenvironment that is not an integral part of a primary functional site, yet are located close to it and are involved in its mechanism of action through non-covalent or dynamic interactions.[1-4] The strategic modification of the secondary sphere can lead to marked increases in the performance of an active site.[5-11] Well explored by enzymes, this principle has been subsequently utilized in a wide range of metal-mediated processes, whereby bioinspired design elements such as distal hydrogen bond donors, electrostatic forces, and hydrophobic binding cavities have been incorporated into the catalyst design.[12-16] Despite the flourishing research, only a handful of reports have explored the association of control over the reactivity of organocatalysts by introducing secondary sphere modifiers, and this is even less in the field of heterogeneous organocatalysis.[17]

With interest in developing catalytic systems for CO_2 transformations, we sought to modify a known organocatalyst, pyridinium salt (an ionic compound with nucleophilic halide counter anions), due to its modularity and wide applications in CO_2 transformations.[18] The key elements to be optimized are increasing the reactivity of the active species and activating the reagent, which allows the reaction to proceed under mild conditions. In order to put these considerations into specific examples, a pyridinium salt was decorated with a library of substitute groups that were employed as building blocks for the construction of cationic porous frameworks. Given the mobility of counter anions, the whole cationic framework can thus be considered as a secondary modifier of the counter anions, through which the reactivity of counter anions could be turned, reminiscent of that seen in the enzyme. The use of porous polymers as a platform is appealing due to the designability and high internal surface areas, which promote a wide range of applications.[19-29] Such modularity allows their compositions to be fine-tuned, thus enabling a rigorous comparison to establish

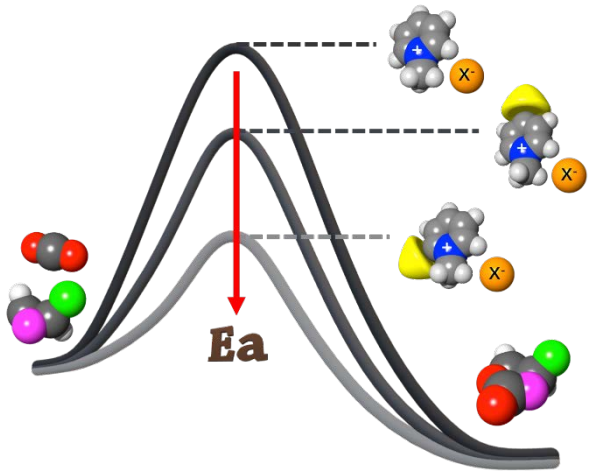

Figure 1. The activation energy diagram for porous polymeric pyridinium salts catalyzed CO_2 transformations. To simplify the figure, only the corresponding pyridinium salt was shown. (grey, C; blue, N; orange, halide anions; yellow, functional group; pink, heteroatom; green, substitute group).

correlations between compositions and the performance of the resulting materials. We postulated that altering the substituted group and its relative position toward the pyridinium motif on the cationic framework would systematically tune the reaction environment of the counter halide anions, and this modification, albeit indirect, would be manifested in the subsequent reactions. Candidate functionalities with various electron-donating/withdrawing strengths and hydrogen bond donor/acceptor, were selected. We then evaluated the consequences in terms of reactivity in CO_2 fixation for the subsequent polymeric pyridinium salts. We found that their activities in the CO_2 transformations are altered, such that the incorporated secondary-sphere modifiers accomplish their tuning not only by indirect electronic communication with the catalytically active species but also by participating in the reagent activation. The performance can be further improved by alternating the relative position of these catalytic relevant elements, as a result of boosted cooperation. In spite of the specifics, our results point to an appealing approach for improving the performance of organocatalytic systems and associated porous catalysts (Figure 1).

RESULTS AND DISCUSSION

Physiochemical and Characterization. In order to investigate whether the reactivity of halide anions could be tuned by tailoring the secondary sphere modifier of the cationic framework, functionalities of -NH_2, -NHCOMe, -$N(Me)_2$, -H, and -Cl were incorporated into a pyridinium motif. To construct these moieties into porous frameworks for easy separation and ready recycling, we installed vinyl groups onto the corresponding functionalized pyridine compounds. To achieve the target polymers, the synthesized monomers and free-radical initiator azobisisobutyronitrile (AIBN) were dissolved in dimethylformamide (DMF). After 24 h of heating at 100 °C, the resulting solids were collected after simple acetone wash, and directly subjected for quaternarization with methyl iodide (CH_3I), followed by ion exchange with NaBr aqueous solution.

The solid-state ^{13}C NMR spectra confirm the transformation from the functionalized pyridine monomers into the respective polymers. This is clearly evident from the emergence of an intense peak attributable to polymerized vinyl groups at around 35.0 ppm, with the concomitant disappearance of resonance of vinyl groups within the range of 110.0 to 120.0 ppm (Figures S1-S6).[30] Whereby, the appearance of the peak at around 45.0 ppm associated with the methyl group from CH_3I, verified the occurrence of the quaternization reaction between the pyridine moiety on these polymers and CH_3I, yielding polymeric quaternary ammonium salts (PQAs). The strong signals of iodine species in the X-ray photoelectron spectroscopy (XPS) spectra of the resulting PQAs at around 629.0 and 617.5 eV for I3$d_{5/2}$ and I3$d_{7/2}$, respectively, provided additional proof of the success of this transformation (Figures S7-S12). The full accessibility of the halide anions within these materials is supported by a complete anion-exchange process between I^- and Br^- with the disappearance of I^- signal as indicated by the XPS analysis. The amount of Br^- ions in the resulting frameworks was quantified by the elemental analysis, revealing that greater than 95% of the pyridine moieties were grafted with the methyl group in all the synthesized materials. To determine the porosity of the resulting polymeric pyridinium-based materials, N_2 sorption isotherms were collected at 77 K, which showed that they processed moderate to high surface areas within the range of 223-477 $m^2\ g^{-1}$ (see summary in Table 1 and Figures S1-S6).

Table 1. Textural parameters of various pyridinium-based porous polymers and the corresponding catalytic activity in the cycloaddition of CO_2 and 1,2-epoxy-3-phenoxypropane.[a]

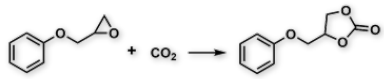

Polymer	Structure	BET ($m^2\ g^{-1}$)	Br content (wt.%)	Yield(%)[b]
PQA-Py-Br		477	33.7	6
PQA-*p*NH_2Py-Br		311	31.6	25
PQA-*p*$N(Me)_2$Py-Br		223	27.8	10
PQA-*p*NHCOMePy-Br		323	27.1	17
PQA-*p*ClPy-Br		327	29.2	5
PQA-*o*NH_2Py-Br		315	30.8	37

[a] Reaction conditions: 1,2-epoxy-3-phenoxypropane (1 g), CO_2 (1 atm), 35 °C, catalyst (25 mg), and reaction for 72 h. [b] The yields were determined by ^1H NMR.

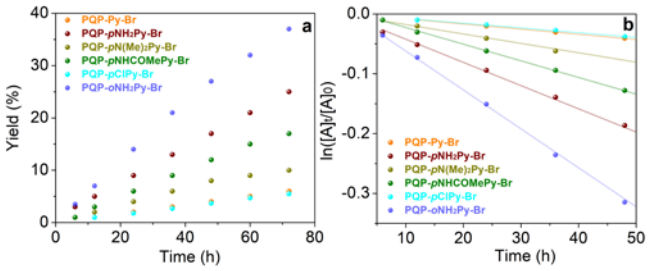

Figure 2. (a) Kinetic rates of carbonate product yields and (b) first-order reaction rate plots (R^2>0.99 for all) over various polymeric pyridinium salts at 35 °C.

Catalytic Performance Investigation. With these materials in hand, we proceed to explore their utility in CO_2 transformations. CO_2 has the potential to be uniquely highly economical as a C1 feedstock due to its being abundant and renewable; however, its inherent thermodynamic stability and kinetic inertness make chemical CO_2 fixation challenging.[31-36] Any efficient reactions for CO_2 fixation are of practical value and would have positive consequences on carbon management. Among the developed reaction routes, the coupling of CO_2 with epoxides to yield cyclic carbonates, a functionality with many industrial relevant applications, has garnered considerable attention.[37-54] To probe the effect of various secondary sphere modifiers on the catalytic performance of Br^- anions in the cycloaddition of CO_2 and epoxides, we initially compared the activity of PQA-*p*NH_2Py-Br and PQA-Py-Br which correspond to the polymeric pyridinium salts with modifiers of -NH_2, and -H, respectively, onto the para position of quaternary ammonium motif. The reactions were carried out with 1 g 1,2-epoxy-3-phenoxypropane and 25 mg catalysts at 35 °C and 1 bar CO_2 in neat. PQA-Py-Br converted 6% of the epoxide, whereas, under otherwise identical conditions, PQA-*p*NH_2Py-Br was more than four-fold superior to that of PQA-Py-Br, offering the carbonate yield of 25% (Table 1, entries 1 and 2). A set of comparative

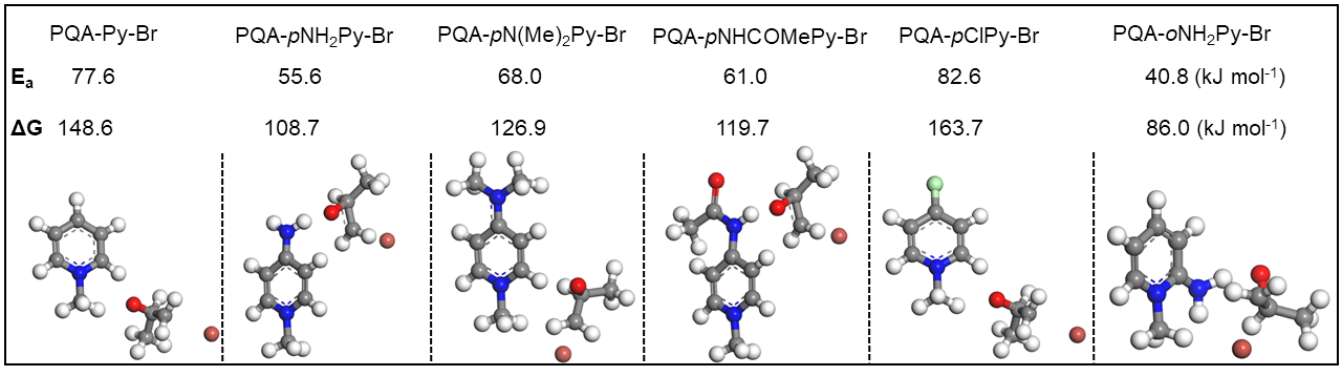

Figure 3. Summary of the apparent activation energies (Ea) in the cycloaddition of 1,2-epoxy-3-phenoxypropane and CO_2 over various polymeric pyridinium salts calculated by Eq.1, and the optimized structures of the ring open step together with the corresponding activation barrier from the ground state to transition state (ΔG) over various molecular pyridinium salts (Py-Br, *p*NH_2Py-Br, *p*$N(Me)_2$Py-Br, *p*NHCOMePy-Br, *p*ClPy-Br, *o*NH_2Py-Br in sequences).

experiments was carried out to rationalize the influence of the amino group in the reaction. To investigate the role of H-bonding interaction, we synthesized a polymeric pyridinium salt with a modifier of -$N(Me)_2$, named as PQA-*p*$N(Me)_2$Py-Br, which lacks the hydrogen bond donor. A sharp drop in activity was detected, giving a 10% conversion of the epoxide (Table 1, entry 3). To explore the electron donating property of the amino group on this transformation, an electron withdrawn group, acetyl group, was placed on the amino group. The resulting material, PQA-*p*NHCOMePy-Br, afforded the 1,2-epoxy-3-phenoxypropane conversion 17% (Table 1, entry 4). To sum up, the reactivity of these pyridinium-based catalysts decreases in the order of PQA-*p*NH_2Py-Br > PQA-*p*NHCOMePy-Br > PQA-*p*$N(Me)_2$Py-Br > PQA-Py-Br.

Given that only a very weak correlation could be established between the catalytic efficiency with the materials' properties in terms of the density of catalytically active species, as well as the material's surface area and CO_2 uptake capacity (Table 1 and Figure S13-S18 and S27-S29), it suggests that these factors are not the dominant paradigm for determining the catalyst performance; instead, the introduced secondary sphere interactions is a more critical factor for the observed discrepancy in catalytic performance. The superior performance of PQA-*p*NH_2Py-Br, PQA-*p*$N(Me)_2$Py-Br, and PQA-*p*NHCOMePy-Br in comparison with the catalyst PQA-Py-Br presumably arises from the equipped electron-donating groups. It weakens the partial positive charge on the cations and facilitates the formation of kinetically labile complexes, allowing for ready Br^- species leaving and consequently higher reactivity. To explain why PQA-*p*NH_2Py-Br and PQA-*p*NHCOMePy-Br outperformed that of PQA-*p*$N(Me)_2$Py-Br, we reasoned that the -NH_2 and -NHCOMe groups act as hydrogen bond donors. Reagents, such as epoxide, are prone to build interaction with the amino/amide group via a hydrogen bond, yielding an activated formulation and thereby facilitating the subsequent transformation. Such explanations can correlate with the following experimental results, wherein the introduction of an electron-withdrawing and non-hydrogen bond donor group, -Cl, gave adverse consequences, with the lowest efficacy among the five materials. The electron-withdrawing property of the -Cl group decreases the leaving ability of the counter anion of pyridinium and hence, reducing its catalytic activity (Table S3). These results thus validate how leveraging outer-sphere engineering to alter the catalytic performance.

As deduced from the results mentioned above, it is envisioned that the relative location of the catalytic elements can lead to diverged outcomes as a result of the "proximity effect," suitable location promoting the cooperation of various catalytic elements and consequently, the accompany reactivity. Satisfied with the positive effect of the amino group on the reaction outcomes, we set out to vary its relative location toward the pyridinium motif. A material with the amino group located in the ortho position of the pyridinium motif was synthesized (PQA-*o*NH_2Py-Br). PQA-*o*NH_2Py-Br outperformed all other catalysts tested with around 1.5-fold superior to that of PQA-*p*NH_2Py-Br (37% vs. 25%), under standard conditions. To further illustrate the superiority of the -NH_2 group on boosting the catalytic efficiency, we treated PQA-*o*NH_2Py-Br with acetyl chloride to yield PQA-*o*NHCOMePy-Br. A decreased carbonate product yield was detected compared to PQA-*o*NH_2Py-Br (22% vs. 37%) under standard conditions. Whereas, the superior performance of PQA-*o*NHCOMePy-Br in comparison with PQA-*p*NHCOMePy-Br further emphasized the location matter of the introduced secondary sphere modifier relative to the catalytic site.

To benchmark the thermodynamic parameters associated with these materials, detailed kinetic studies were performed in the range of 35 °C to 50 °C. The conversion of 1,2-epoxy-3-phenoxypropane steadily increased over time at all temperatures, and the apparent influence of temperature on the reaction rate was observed, increasing along with reaction temperature. The reactions are first order, as demonstrated by the fact that all the catalytic data show excellent fits to the linear plot of the natural logarithm of the epoxide concentration against time (t) with correlation coefficients (R^2) approximately equal to 1 (Figure 2). The pseudo-first-order rate constant k values of PQA-*o*NH_2Py-Br derived from the slopes are 0.00646, 0.00833, and 0.0135 s^{-1}, at 35 °C, 40 °C, and 50 °C, respectively (Table S1). By increasing the temperature to 120 °C, the reaction proceeded to completion within 12 h at a substrate to catalyst ratio of 1000, placing it on par with the most active heterogeneous organocatalyst for CO_2 transformation (Table S2).[37-54] PQA-*o*NH_2Py-Br showed higher reaction rates at all temperatures evaluated in comparison with

other material tested under the otherwise identical conditions (Figures 2a and S19).

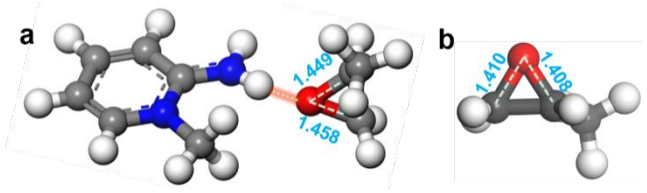

Figure 4. (a) Hydrogen bonding interaction between the amine group on the cationic moiety of PQA-*o*NH_2Py-Br and propylene oxide (atom colors in geometries: C: gray, N: blue, O: red, H: white) and the comparisons of C-O bond lengths in propylene oxide (b) and that with the hydrogen bonding interaction with the amine group (a). The unit of bond length is Å.

Using the Arrhenius equation (Eq 1), the apparent activation energy (E_a) was calculated by fitting the data from a plot of the natural logarithm of the rate constant (lnk) against the reciprocal of the absolute temperature (1/T). In the temperature range of 35 °C-50 °C, PQA-*o*NH_2Py-Br, PQA-*p*NH_2Py-Br, PQA-*p*NHCOMePy-Br, PQA-*p*$N(Me)_2$Py-Br, PQA-Py-Br, and PQA-*p*ClPy-Br exhibit E_a values of 40.8, 55.6, 61.0, 68.0, 77.6, and 82.6 kJ mol^{-1}, respectively (Figures 3 and S20). This indicates that less energy is required for PQA-*o*NH_2Py-Br compared to other materials studied to achieve the same outcome, confirming the advantages of equipping amino group proximity to the pyridinium motif; with the enhanced cooperation between these two catalytic elements reduces the energy barrier required and improves efficiency.

$$E_a = \mathrm{Rln}\left(\frac{k_2}{k_1}\right) / \left(\frac{1}{T_1} - \frac{1}{T_2}\right) \qquad \text{Eq. 1}$$

DFT Calculations. To gain an insight into the diverged reaction outcomes for the catalytic materials with various secondary sphere modifiers, DFT calculations were performed according to the established reaction pathway. To simplify the calculation, the pyridinium salt moieties and propylene oxide were used as the models for catalysts and reagents, respectively. The most stable transition-state structures in the rate-determining step (ring-opening) along with the predicted free energy profiles catalyzed by these pyridinium salt moieties are displayed in Figure 3.[45] The hydrogen bonding interaction between the amino group and the O species in propylene oxide was observed, as reflected by the enlargement of the C-O bond,

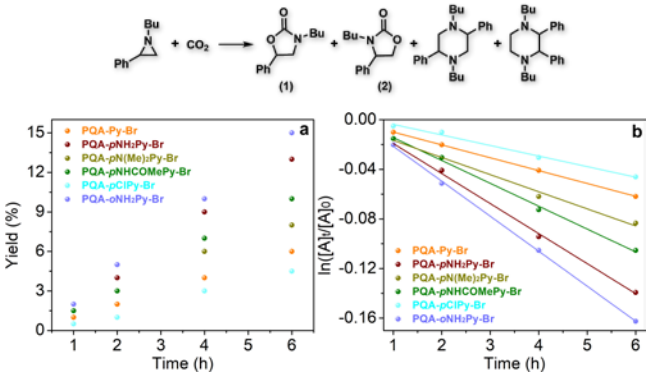

Figure 5. (a) Kinetic rates of oxazolidinone product yields and (b) first-order reaction rate plots (R^2>0.99 for all) over various polymeric pyridinium salts at 40 °C. Reaction conditions: 1-butyl-2-phenyl aziridine (175 mg, 1 mmol), CO_2 (1 MPa), catalyst (5 mg), and reaction for 6 h. The yields and the selectivity were determined by ^{1}H NMR. All catalysts gave the oxazolidinone products selectivity higher than 99%.

which facilitates the following bromohydrin formation (Figure 4). To validate this experimentally, Fourier transform infrared (FT-IR) analysis was carried out, showing that the C-O vibration in the epoxide compound shifted from 1133 cm^{-1} to 1129 cm^{-1} after association with PQA-*o*NH_2Py-Br and concurrently, the N-H vibration shifted to 3345 cm^{-1} from the pristine PQA-*o*NH_2Py-Br (3338 cm^{-1}, Figure S21). The activation barrier from the ground state to the transition state of the pyridinium moieties decreased in the order of *p*ClPy-Br (163.7 kJ mol^{-1}) > Py-Br (148.6 kJ mol^{-1}) > *p*$N(Me)_2$Py-Br (126.9 kJ mol^{-1}) > *p*NHCOMePy-Br (119.7 kJ $mol^{-1)}$ > *p*NH_2Py-Br (108.7 kJ mol^{-1}) > *o*NH_2Py-Br (86.0 kJ mol^{-1}), which is in well agreement with the experimental trends (Figure 3). According to these experimental results and the literature reports, a tentative mechanism was proposed (Figure S22).

With the optimal material of PQA-*o*NH_2Py-Br, we further investigated its substrate tolerance. The catalyst system was found to be applicable to a variety of epoxides, and all offered the corresponding carbonate products in excellent yields with only a slight difference in reaction rate (Table S4). The catalyst showed excellent recyclability with fully retained activity for at least ten cycles (Table S5). Moreover, the structure integrity of catalyst was maintained in this process, as revealed by IR analysis and N_2 sorption (Figures S23 and S24). To determine the heterogeneity of the detected activity, we monitored the potential Br^- ions leaching by a hot filtration experiment and found no detectable increase in the yield of the carbonate product for the resulting filtrate.

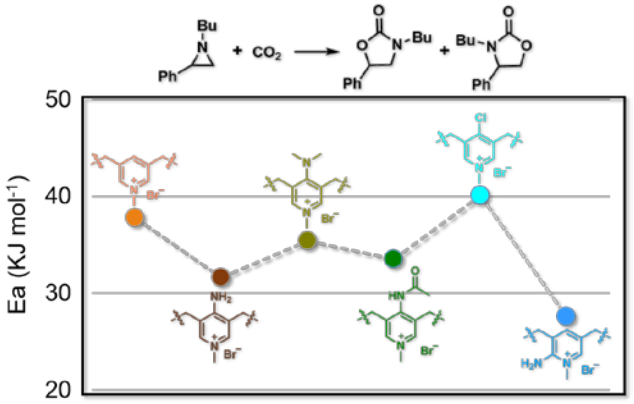

Figure 6. Reaction scheme of the cycloaddition of CO_2 and1-butyl-2-phenyl aziridine and the calculated activation energies over various polymeric pyridinium salts (see detailed experimental procedures in the Supporting Information).

Advantageously, our strategy of tailoring the secondary-sphere modifiers to promote catalyst reactivity is also readily extended to other reactions. To showcase this, we applied these materials in the cycloaddition of aziridines and CO_2,[55-58] showing that the performance of the Br^- anions followed the same trend as that observed in the coupling of epoxides and CO_2. PQA-*o*NH_2Py-Br outperformed all other materials evaluated in terms of reaction rate (Figures 5, S25, and S26, and Table S6). Specifically, the pseudo-first-order rate constant k values derived from the slopes of the reaction rate plots are 0.01037, 0.02422, 0.01381, 0.01845, 0.00852 and 0.02823 s^{-1} for PQA-Py-Br, PQA-*p*NH_2Py-Br, PQA-*p*$N(Me)_2$Py-Br, PQA-

*p*NHCOMePy-Br, PQA-*p*ClPy-Br, and PQA-*o*NH_2Py-Br, respectively, at 40 °C (Figure 5b). Concretely, the activation energy increased in the order of PQA-*p*ClPy-Br (40.1 kJ mol^{-1}) > PQA-Py-Br (37.8 kJ mol^{-1}) > PQA-*p*$N(Me)_2$Py-Br (35.4 kJ mol^{-1}) > PQA-*p*NHCOMePy-Br (33.5 kJ mol^{-1}) > PQA-*p*NH_2Py-Br (31.6 kJ mol^{-1}) > PQA-*o*NH_2Py-Br (27.6 kJ mol^{-1}), as shown in Figure 6.

EXPERIMENTAL SECTION

Synthesis of polymeric pyridinium salt. Under solvothermal conditions in dimethylformamide (DMF) at 100 °C, various vinyl functionalized pyridine-based monomers were polymerized in the presence of azobisisobutyronitrile (AIBN) as a free radical initiator. The resulting polymers were treated with methyl iodide (CH_3I), followed by ion exchange with NaBr aqueous solutions (Figures S30-S38).

Catalytic tests. *Cycloaddition reactions of epoxides and CO_2:* 1 g of epoxide and 25 mg of catalyst were introduced into a 10 mL Schlenk flask. The resulting system was vacuum-sealed and then purged with CO_2 by adding a balloon. The tube was then placed in a preheated oil bath and allowed to stir for a designated time interval. The carbonate product yields were analyzed by ^{1}H NMR (Figures S39, S41, and S42). For the recycling test, the catalyst was separated from the reaction system by centrifugation, washed with $CHCl_3$ for three times, and dried. The resulting polymer was used directly for the next catalytic evaluation.

Coupling of aziridines and CO_2: A 7 mL vial charged with1 mmol of aziridines and 5 mg of catalyst was placed into a 100 mL stainless steel autoclave. After being sealed, the autoclave was purged with CO_2 to 1 MPa. The autoclave was then placed in a preheated oil bath and allowed to stir for a designated time interval. The oxazolidinone product yields were analyzed by ^{1}H NMR using terephthalaldehyde as an internal standard (Figures S40, S43, and S44).

CONCLUSION

In summary, we investigate in detail how secondary sphere variations affect the reactivity of organocatalysts toward CO_2 transformations through perturbation of the reactivity of the active sites and activation of the reagents. A library of substituted groups with changes in the electronic property and the hydrogen bond donating ability was studied to tailoring the properties of the polymeric pyridinium cationic framework, demonstrating that the reactivity of the counter anions can be optimized. It was also found that such effects on reactions are position-dependent. Given the significantly accelerated kinetics by a factor over six times, the strategy presented herein provides an alternative route to the current ones that usually call for the cumbersome development of new active sites. Therefore, rational modification of the outer-sphere should accelerate improvements of catalysts and can serve as a roadmap for future synthesis of highly efficient catalytic materials.

ASSOCIATED CONTENT

Supporting Information. Material synthesis; Characterization details; IR, NMR, XPS; DFT calculations; and supporting figures. This material is available free of charge via the Internet at http://pubs.acs.org.

AUTHOR INFORMATION

Corresponding Author

sqma@usf.edu (SM)
sunqichs@zju.edu.cn (QS)

Notes

The authors declare no competing financial interest.

ACKNOWLEDGMENT

The authors thank the financial support for this work from the US National Science Foundation (DMR-1352065) and the University of South Florida.

REFERENCES

1. Cook, S. A.; Borovik, A. S. Molecular Designs for Controlling the Local Environments Around Metal Ions. *Acc. Chem. Rev.* **2015**, *48*, 2407-2414.
2. Reedijk, J. Coordination Chemistry beyond Werner: Interplay between Hydrogen Bonding and Coordination. *Chem. Soc. Rev.* **2013**, *42*, 1776-1783.
3. Dhayalan, V; Gadekar, S. C.; Alassad, Z.; Milo, A. Unravelling Mechanistic Features of Organocatalysis with in situ Modifications at the Secondary Sphere. *Nat. Chem.* **2019**, *11*, 543-551.
4. Slater, J. W.; Marguet, S. C.; Gray, M. E.; Monaco, H. A.; Sotomayor, M.; Shafaat, H. S. Power of the Secondary Sphere: Modulating Hdrogenase Activity in Nickel-Substituted Rubredoxin. *ACS Catal.* **2019**, *9*, 8928-8942.
5. Hale, L. V. A.; Szymczak, N. K. Hydrogen Transfer Catalysis beyond the Primary Coordination Sphere. *ACS Catal.* **2018**, *7*, 6446-6461.
6. Wallen, C. M.; Palatinus, L.; Bacsa, J.; Scarborough, C. C. Hydrogen Peroxide Coordination to Cobalt(II) Facilitated by Second-Sphere Hydrogen Bonding. *Angew. Chem. Int. Ed.* **2016**, *55*, 11902-11906.
7. Sun, Q.; Wang, S.; Aguila, B.; Meng, X.; Ma, S.; Xiao, F.-S. Creating Solvation Environments in Heterogeneous Catalysts for Efficient Biomass Conversion. *Nat. Commun.* **2018**, *9*, 3236.
8. Gesslbauer, S.; Savela, R.; Chen, Y.; White, A. J. P.; Romain, C. Exploiting Noncovalent Interactions for Room-Temperature Heteroselective *rac*-Lactide Polymerization Using Aluminum Catalysts. *ACS Catal.* **2019**, *9*, 7912-7920.
9. Sun, Q.; Tang, Y.; Aguila, B.; Wang, S.; Xiao, F.-S.; Thallapally, P. K.; Al-Enizi, A. M.; Nafady, A.; Ma, S. Reaction Environment Modification in Covalent Organic Frameworks for Catalytic Performance Enhancement. *Angew. Chem. Int. Ed.* **2019**, *58*, 8670-8675.
10. Zhao, M.; Yuan, K.; Wang, Y.; Li, G.; Guo, J.; Gu, L.; Hu, W.; Zhao, H.; Tang, Z. Metal-Organic Frameworks as Selectivity Regulators for Hydrogenation Reactions. *Nature* **2016**, *539*, 76-80.
11. Davis, H. J, Phipps, R. J. Harnessing Non-Covalent Interactions to Exert Control over Regioselectivity and Site-Selectivity in Catalytic Reactions. *Chem. Sci.* **2017**, *8*, 864-877.
12. Toste, F. D.; Sigman, M. S.; Miller, S. J. Pursuit of Noncovalent Interactions for Strategic Site-Selective Catalysis. *Acc. Chem. Res.* **2017**, *50*, 609-615.
13. Meeuwissen, J.; Reek, J. N. H. Supramolecular Catalysis beyond Enzyme Mimics. *Nat. Chem.* **2010**, *2*, 615-621.
14. Grosso-Giordano, N. A.; Schroeder, C.; Okrut, A.; Solovyov, A.; Schöttle, C.; Chassé, W.; Marinković, N.; Koller, H.; Zones, S. I.; Katz, A. Outer-Sphere Control of Catalysis on Surfaces: A Comparative Study of Ti(IV) Single-Sites Grafted on Amorphous Versus Crystalline Silicates for Alkene Epoxidation. *J. Am. Chem. Soc.* **2018**, *140*, 4956-4960.
15. Xiao, D. J.; Oktawiec, J.; Milner, P. J.; Long, J. R. Pore Environment Effects on Catalytic Cyclohexane Oxidation in Expanded Fe_2(dobdc) Analogues. *J. Am. Chem. Soc.* **2016**, *138*, 14371-14379.

16. Szécsénui, Á.; Khramenkova, E.; Chernyshov, I. Y.; Li, G.; Gascon, J.; Pidko, E. A. Breaking Linear Scaling Relationships with Secondary Interactions in Confined Space: A Case Study of Methane Oxidation by Fe/ZSM-5 Zeolite. *ACS Catal*. **2019**, *9*, 9276-9284.
17. Liu, L.; Zhou, T.-Y.; Telfer, S. G. Modulating the Performance of An Asymmetric Organocatalyst by Tuning its Spatial Environment in A Metal-Organic Framework. *J. Am. Chem. Soc*. **2017**, *139*, 13936-13943.
18. Sun, X.; Luo, H.; Dai, S. Ionic Liquids-Based Extraction: A Promising Srategy for the Advanced Nuclear Fuel Cycle. *Chem. Rev*. **2012**, *112*, 2100-2128.
19. Slater, A. G.; Cooper, A. I. Function-Led Design of New Porous Materials. *Science* **2015**, *348*, aaa8075.
20. Das, S.; Heasman, P.; Ben, T.; Qiu, S. Porous Organic Materials: Strategic Design and Structure-Function Correlation. *Chem. Rev*. **2017**, *117*, 1515-1563.
21. Xu, Y.; Jin, S.; Xu, H.; Nagai, A.; Jiang, D. Conjugated Microporous Polymers: Design, Synthesis and Application. *Chem. Soc. Rev*. **2013**, *42*, 8012-8031.
22. Wu, D.; Xu, F.; Sun, B.; Fu, R.; He, H.; Matyjaszewski, K. Design and Preparation of Porous Polymers. *Chem. Rev*. **2012**, *112*, 3959-4015.
23. Ben, T.; Pei, C.; Zhang, D.; Xu, J.; Deng, F.; Jing, X.; Qiu, S. Gas Storage in Porous Aromatic Frameworks (PAFs). *Energy Environ. Sci*. **2011**, *4*, 3991-3999.
24. Yan, Z.; Yuan, Y.; Tian, Y.; Zhang, D.; Zhu, G. Highly Efficient Enrichment of Volatile Iodine by Charged Porous Aromatic Frameworks with Three Sorption Sites. Angew. Chem. Int. Ed. **2015**, *54*, 12733-12737.
25. Sun, Q.; Aguila, B.; Perman, J.; Ivanov, A. S.; Bryantsev, V. S.; Earl, L. D.; Abney, C. W.; Wojtas, L.; Ma, S. Bio-Inspired Nano-Traps for Uranium Extraction from Seawater and Recovery from Nuclear Waste. *Nat. Commun*. **2018**, *9*, 1644.
26. Alsbaiee, A.; Smith, B. J.; Xiao, L.; Ling, Y.; Helbling, D. E.; Dichtel, W. R. Rapid Removal of Organic Micropollutants from Water by A Porous β-Cyclodextrin Polymer. *Nature* **2016**, *529*, 190-194.
27. Chaoui, N.; Trunk, M.; Dawson, R.; Schmidt, J.; Thomas, A. Trends and Challenges for Microporous Polymers. *Chem. Soc. Rev*. **2017**, *46*, 3302-3321.
28. Sun, J.-K.; Antonietti, M.; Yuan, J. Nanoporous Ionic Organic Networks: From Synthesis to Materials Applications. *Chem. Soc. Rev*. **2016**, *45*, 6627-6656.
29. Yu, X.; Yang, Z.; Qiu, B.; Guo, S.; Yang, P.; Yu, B.; Zhang, H.; Zhao, Y.; Yang, X.; Han, B.; Liu, Z. Eosin Y-Functionalized Conjugated Organic Polymers for Visible-Light-Driven CO_2 Reduction with H_2O to CO with High Efficiency. *Angew. Chem. Int. Ed*. **2019**, *58*, 632-636.
30. Sun, Q.; Zhu, L.; Aguila, B.; Thallapally, P. K.; Xu, C.; Chen, J.; Wang, S.; Rogers, D.; Ma, S. Optimizing Radionuclide Sequestration in Anion Nanotraps with Record Pertechnetate Sorption. *Nat. Commun*. **2019**, *10*, 1646.
31. Huang, K.; Zhang, J.-Y.; Liu, F.; Dai, S. Synthesis of Porous Polymeric Catalysts for the Conversion of Carbon Dioxide. *ACS Catal*. **2018**, *8*, 9079-9102.
32. Liu, Q.; Wu, L.; Jackstell, R.; Beller, M. Using Carbon Dioxide as A Building Block in Organic Synthesis. *Nat. Commun*. **2015**, *6*, 5933.
33. Chen, G.; Waterhouse, G. I. N.; Shi, R.; Zhao, J.; Li, Z.; Wu, L.-Z.; Tung, C.-H.; Zhang, T. From Solar Energy to Fuels: Recent Advances in Light-Driven C_1 Chemistry. *Angew. Chem. Int. Ed*. **2019**, *58*, 17528-17551.
34. Hulla, M.; Dyson, P. J. Pivotal Role of the Basic Character of Organic and Salt Catalysts in C-N Bond Forming Reactions of Amines with CO_2. *Angew. Chem. Int. Ed*. **2020**, *59*, 1002-1017.
35. Moore, D. R.; Cheng, M.; Lobkovsky, E. B.; Coates, G. W. Mechanism of the Alternating Copolymerization of Epoxides and CO_2 Using β-Diiminate Zinc Catalysts: Evidence for A Bimetallic Epoxide Enchainment. *J. Am. Chem. Soc*. **2003**, *125*, 11911-11924.
36. Hu, J.; Ma, J.; Zhu, Q.; Zhang, Z.; Wu, C.; Han, B. Transformation of Atmospheric CO_2 Catalyzed by Protic Ionic Liquids: Efficient Synthesis of 2-Oxazolidinones. *Angew. Chem. Int. Ed*. **2015**, *54*, 5399-5403.
37. Gao, W.-Y.; Chen, Y.; Niu, Y.; Williams, K.; Cash, L.; Perez, P. J.; Wojtas, L.; Cai, J.; Chen, Y.-S.; Ma, S. Crystal Engineering of an nbo Topology Metal-Organic Framework for Chemical Fixation of CO_2 under Ambient Conditions. *Angew. Chem. Int. Ed*. **2014**, *53*, 2615-2619.
38. Xie, Y.; Wang, T.-T.; Liu, X.-H.; Zou, K.; Deng, W.-Q. Capture and Conversion of CO_2 at Ambient Conditions by A Conjugated Microporous Polymer. *Nat. Commun*. **2013**, *4*, 1960.
39. Desens, W.; Kohrt, C.; Frank, M.; Werner, T. Highly Efficient Polymer-supported Catalytic System for the Valorization of Carbon Dioxide. *ChemSusChem* **2015**, *8*, 3815-3822.
40. Maeda, C.; Taniguchi, T.; Ogawa, K.; Ema, T. Bifunctional Catalysts Based on *m*-Phenylene-Bridged Porphyrin Dimer and Trimer Platforms: Synthesis of Cyclic Carbonates from Carbon Dioxide and Epoxides. *Angew. Chem. Int. Ed*. **2015**, *54*, 134-138.
41. Whiteoak, C. J.; Kielland, N.; Laserna, V.; Escudero-Adán, E. C.; Martin, E.; Kleij, A. W. A Powerful Aluminum Catalyst for the Synthesis of Highly Functional Organic Carbonates. *J. Am. Chem. Soc*. **2013**, *135*, 1228-1231.
42. Dai, Z.; Sun, Q.; Liu, X.; Bian, C.; Wu, Q.; Pan, S.; Wang, L.; Meng, X.; Deng, F.; Xiao, F.-S. Metalated Porous Porphyrin Polymers as Efficient Heterogeneous Catalysts for Cycloaddition of Epoxides with CO_2 under Ambient Conditions. *J. Catal*. **2016**, *338*, 202-209.
43. Sun, Q.; Jin, Y.; Aguila, B.; Meng, X.; Ma, S.; Xiao, F.-S. Porous Ionic Polymers as a Robust and Efficient Platform for Capture and Chemical Fixation of Atmospheric CO_2. *ChemSusChem* **2017**, *10*, 1160-1165.
44. Dong, J.; Cui, P.; Shi, P.-F.; Cheng, P.; Zhao, B. Ultrastrong Alkali-Resisting Lanthanide-Zeolites Assembled by $[Ln_{60}]$ Nanocages. *J. Am. Chem. Soc*. **2015**, *137*, 15988-15991.
45. Beyzavi, M. H.; Klet, R. C.; Tussupbayev, S.; Borycz, J.; Vermeulen, N. A.; Cramer, C. J.; Stoddart, J. F.; Hupp, J. T.; Farha, O. K. A Hafnium-Based Metal-Organic Framework as an Efficient and Multifunctional Catalyst for Facile CO_2 Fixation and Regioselective and Enantioretentive Epoxide Activation. *J. Am. Chem. Soc*. **2014**, *136*, 15861-15864.
46. Li, P.-Z.; Wang, X.-J.; Liu, J.; Lim, J. S.; Zou, R.; Zhao, Y. A Triazole-Containing Metal-Organic Framework as a Highly Effective and Substrate Size-Dependent Catalyst for CO_2. *J. Am. Chem. Soc*. **2016**, *138*, 2142-2145.
47. Zhou, Z.; He, C.; Xiu, J.; Yang, L.; Duan, C. Metal-Organic Polymers Containing Discrete Single-Walled Nanotube as A Heterogeneous Catalyst for the Cycloaddition of Carbon Dioxide to Epoxides. *J. Am. Chem. Soc*. **2015**, *137*, 15066-15069.
48. Sun, Q.; Aguila, B.; Perman, J.; Nguyen, N.; Ma, S. Flexibility Matters: Cooperative Active Sites in Covalent Organic Framework and Threaded Ionic Polymer. *J. Am. Chem. Soc*. **2016**, *138*, 15790-15796.
49. Feng, D.; Chung, W.-C.; Wei, Z.; Gu, Z.-Y.; Jiang, H.-L.; Y.-P. Chen, Y.-P.; Darensbourg, D. J.; Zhou, H.-C. Construction of Ultrastable Porphyrin Zr Metal-Organic Frameworks through Linker Elimination. *J. Am. Chem. Soc*. **2013**, *135*, 17105-17110.
50. Li, H.; Li, C.; Chen, J.; Liu, L.; Yang, Q. Synthesis of A Pyridin-zinc-based Porous Organic Polymer for the Co-Catalyst-Free Cycloaddition of Epoxides. *Chem. Asian J*. **2017**, *12*, 1095-1103.
51. Liu, Y.-X.; Wang, H.-H.; Zhao, T.-J.; Zhang, B.; Su, H.; Xue, Z.-H.; Li, X.-H.; Chen, J.-S. Schottky Barrier Induced Coupled Interface of Electron-Rich n-Doped Carbon and Electron-Deficient Cu: In-Built Lewis Acid-Base Pairs for Highly Efficient CO_2 Fixation. *J. Am. Chem. Soc*. **2019**, *141*, 38-41.
52. Liang, L.; Liu, C.; Jiang, F.; Chen, Q.; Zhang, L.; Xue, H.; Jiang, H.-L.; Qian, J.; Yuan, D.; Hong, M. Carbon Dioxide Capture and Conversion by An Acid-base Resistant Metal-Organic Framework. *Nat. Commun*. **2017**, *8*, 1233.
53. Ji, G.; Yang, Z.; Zhang, H.; Zhao, Y.; Yu, B.; Ma, Z.; Liu, Z. Hierarchically Mesoporous *o*-Hydroxyazobenzene Polymers:

Synthesis and Their Applications in CO_2 Capture and Conversion. *Angew. Chem. Int. Ed.* **2016**, *55*, 9685-9689.

54. Mu, Z.-J.; Ding, X.; Chen, Z.-Y.; Han, B.-H. Zwitterionic Covalent Oganic Frameworks as Catalysts for Herarchical Reduction of CO_2 with Amine and Hydrosilane. *ACS Appl. Matter. Interfaces* **2018**, *10*, 41350-41358.
55. Xu, H.; Liu, X.-F.; Cao, C.-S.; Zhao, B.; Cheng, P.; He, L.-N. A Porous Metal-Organic Framework Assembled by $[Cu_{30}]$ Nanocages: Serving as Recyclable Catalysts for CO_2 Fixation with Aziridines. *Adv. Sci*. **2016**, *3*, 1600048.
56. Barbachyn, M. R.; Ford, C. W. Oxazolidinone Structure-Activity Relationships Leading to Linezolid. *Angew. Chem. Int. Ed*. **2003**, *42*, 2010-2023.
57. Wang, X.; Gao, W.-Y.; Niu, Z.; Woktas, L.; Perman, J. A.; Chen, Y.-S.; Li, Z.; Aguila, B.; Ma, S. A Metal-Metalloporphyrin Framework Based on An Octatopic Porphyrin Ligand for Chemical Fixation of CO_2 with Aziridines. *Chem. Commun.* **2018**, *54*, 1170-1173.
58. Song, Y.; Sun, Q.; Aguila, B.; Ma, S. Optimizing the Performance of Porous Pyridinium Frameworks for Carbon Dioxide Transformation. *Catal. Today* **2020**, doi.org/10.1016/j.cattod.2020.01.031.

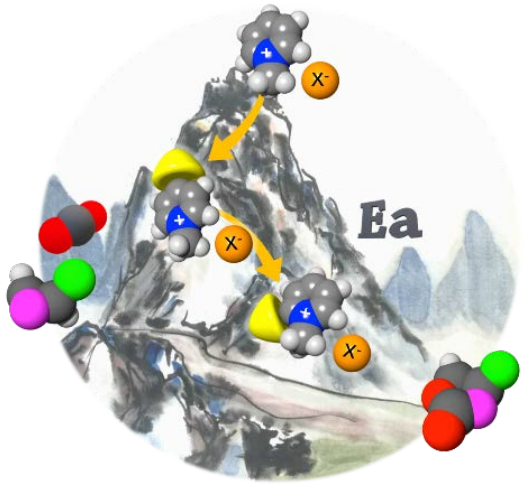
X-
X-
X-
Ea